A Single-Input Two-Output Feedback Formulation for ANC Problems

V. Toochinda[‡1], T. Klawitter[‡], C.V. Hollot[†] and Y. Chait[‡]
‡MIE Department, †ECE Department, University of Massachusetts, Amherst, MA 01003

Abstract

This paper explores inherent feedback limitations of active noise control in ducts by using a single-input, two-output framework and observing properties of closed-loop transfer functions. Performance is assessed using the plant and disturbance alignment angle. We show that the sound levels at the measurement microphone are amplified when attenuating acoustic energy at the error microphone. We also show that the stability margins can be improved over feedforward control using measurements from two sensors.

1 Introduction

In recent years, the potential benefit of using active noise control (ANC) in commercial applications has driven recent academic research; e.g., see [1] and [2]. In contrast to passive techniques, a typical ANC scheme uses additional secondary sources and adaptive algorithms to cancel noise from the original primary source by, roughly speaking, introducing "anti-noise" - an exact but out-of-phase copy of the noise. The level of cancellation depends critically on the ability to produce such anti-noise in the face of uncertain system dynamics and noise properties. Such is the motivation for the introduction of adaptive cancellation techniques [1] as well as the more recent feedforward/feedback methods [3, 4, 6].

This paper is a continuation of some of our previous work [3]-[6] where we explore the use of non-adaptive, fixed-filter schemes for ANC in ducts. Our motivation for using fixed-filters lies in the simplicity of implementation and availability of tools for analyzing stability and performance. Other work using the non-adaptive approach can be found in [7] and [8] and the references contained therein.

The main goal of this paper is to analyze a non-adaptive ANC design reported in [4], within the framework of single-input, two-output (SITO) feedback control previously developed in [9]. This design used two sensors (measurement and error microphones) and a so-called feedforward/feedback configuration. In Section 3 we will show that the placement of the secondary source, relative to the disturbance source, plays an important role in performance. In particular, we will demonstrate, via analysis and examination of experimental data collected in [4], that noise attenuation at the error microphone must come at the expense of amplification at the measurement microphone. We believe this is the first time this observation is made in the literature. Our second result, discussed in Section 4, argues that the role of feedback in ANC is not for noise attenuation, but for stability robustness. In Section 2 we begin our discussion by describing the ANC duct setup and the design results of [4].

2 Description of ANC setup and design results

Figure 1 illustrates a basic configuration of an active noise control problem. It consists of a duct with two loudspeakers and two microphones mounted on it. The speaker located upstream simulates a disturbance source that injects acoustic "noise" into the duct. A measurement microphone detects the disturbance near the source and the downstream error microphone measures the level of noise cancellation at a point in the duct where noise attenuation is desired. The ANC system uses the information provided by these two microphones to generate a signal and send it to the canceling loudspeaker. The objective of the controller is to minimize the acoustic energy at the error microphone. In the ANC literature, the action taken on the measurement microphone signal y_m is referred to as "feedforward" [1] control, while action taken on y_e is called "feedback" control. While such terminology can be ambiguous in the presence of acoustic feedback, we will nevertheless retain this terminology for sake of consistency. The ANC configuration used in [4] is similar to that shown in Figure 1. The measurement microphone is colocated with the disturbance source, and the cancelling speaker is colocated with the error microphone. The duct-length is about one meter with a diameter of 0.1 meters. The two microphones are separated by

[1] The first author is supported by Faculty of Engineering, Kasetsart University, Thailand.
Email: vtoochin@acad.umass.edu

[1] The term feedforward comes from the fact that the measurement microphone is located upstream i.e. closer to the disturbance source. Unlike a conventional feedforward control, however, the acoustic feedback from the control speaker could affect closed-loop stability.

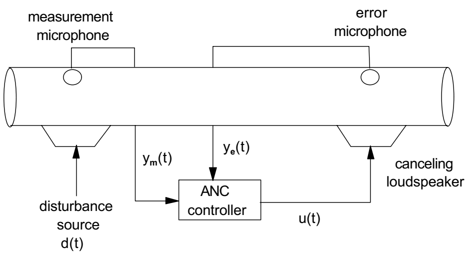

Figure 1: ANC system in a duct.

approximately 0.8 meters of duct. Motivation for this placement of measurement microphone and cancelling speaker came from [8], where only y_m was considered as input to their ANC controller. Interestingly, we will see in Section 3 (see Remark 1) that it may be preferrable to reconsider colocating the cancelling speaker with the disturbance – a configuration not recommended in [8].

With the configuration shown in Figure 1, a formal design of feedforward and feedback controllers was executed in [4] using both H_∞ synthesis and QFT loop-shaping techniques. A comparison of the experimental open and closed-loop performance is shown in Figure 2. This figure plots the magnitude frequency response of y_e due to sinusoidal excitation at d. Note that this ANC design achieves broadband attenuation from approximately 180 - 1000 Hz with no amplification below 2000 Hz. Our subsequent analysis is driven by a desire to understand the roles of feedforward and feedback in this particular design.

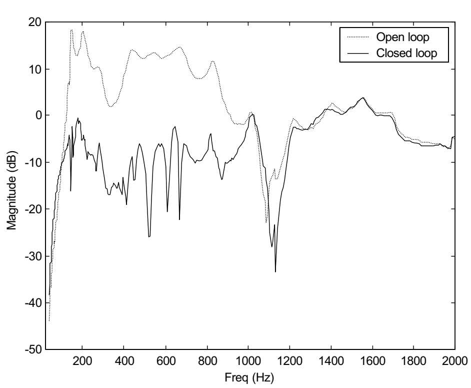

Figure 2: Comparison of open loop and closed-loop frequency response

Our empical observations were twofold:

1. While noise attenuation was achieved at y_e, as shown in Figure 2, amplification occurs at y_m. In the next section, we will show why this occurs and prove that this amplification is not a function of the structure or value of the controllers, but is due to the duct dynamics coupled with the location of the microphones and placement of the cancelling speaker.

2. The feedback controller C_e did not contribute to the level of noise attenuation achieved at y_e – this was primarily accomplished by the feedforward controller C_m. Indeed, the attenuation curve in Figure 2 is only slightly perturbed when we switched-out C_e. However, the *robustness* of this performance to variations in C_m were significantly improved by the presence of the feedback element C_e.

3 Performance analysis

In this section we analyze the performance of the ANC design in [4]. We start by treating the duct (or plant) as a SITO system $\mathbf{P}(s)$ where the input is the canceling speaker input u and the outputs are the microphone signals y_m and y_e, respectively. Conversely, we view the controller as a two-input, single-output system $\mathbf{C}(s)$ with inputs y_m and y_e and output u. Their interconnection forms the feedback control system shown in Figure 3. The objective of this section is to analyze the performance in y_m and y_e. We will show that y_e is attenuated at the expense of amplified y_m. Most importantly, this finding will be shown independent of the value or structure of the controllers (as long as y_e is attenuated). It will depend only on the configuration of microphones and canceling speakers.

To start, consider Figure 3, where $P_{ed}(s)$, $P_{eu}(s)$, $P_{md}(s)$, and $P_{mu}(s)$ are the transfer functions from the disturbance speaker to the error microphone, the canceling speaker to the error microphone, the disturbance speaker to the measurement microphone, and the canceling speaker to the measurement microphone, respectively. Let $C_m(s)$ denote the *feedforward* controller and $C_e(s)$ the *feedback* controller. Further, define the plant, controller, and disturbance transfer functions as:

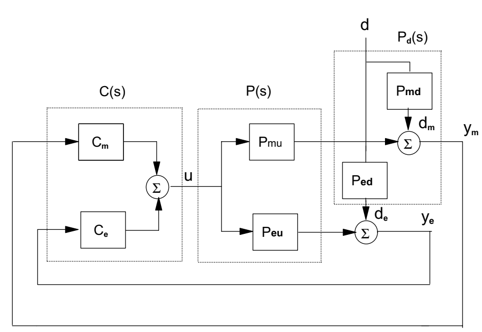

Figure 3: ANC as a single input, two output feedback system

$$\mathbf{P}(s) \triangleq \begin{bmatrix} P_{mu}(s) \\ P_{eu}(s) \end{bmatrix}; \qquad \mathbf{C}(s) \triangleq \begin{bmatrix} C_m(s) & C_e(s) \end{bmatrix}.$$

$$\mathbf{P}_d(s) \triangleq \begin{bmatrix} P_{md}(s) \\ P_{ed}(s) \end{bmatrix}$$

Assume zero input and initial conditions for the plant transfer function, the open loop response is then

$$y(s)_{OL} \triangleq \begin{bmatrix} y_m(s) \\ y_e(s) \end{bmatrix} = \mathbf{P}_d(s)d(s).$$

Associated with this feedback system are several important transfer functions. These are the input and output loop transfer functions: $L_I(s) = \mathbf{C}(s)\mathbf{P}(s)$ and $\mathbf{L}_O(s) = \mathbf{P}(s)\mathbf{C}(s)$, the input and output sensitivity functions: $S_I(s) = (1 + L_I(s))^{-1}$ and $\mathbf{S}_O(s) = (\mathbf{I} + \mathbf{L}_O(s))^{-1}$, and the input and output complementary sensitivity functions: $T_I(s) = L_I(s)(1 + L_I(s))^{-1}$ and $\mathbf{T}_O(s) = \mathbf{L}_O(s)(I + \mathbf{L}_O(s))^{-1}$. The dimension of transfer functions at the plant input are 1x1, while those at the plant output are 2 x 2 . In our context, the closed-loop response of interest is:

$$y(s)_{CL} = \mathbf{S}_O(s) \begin{bmatrix} d_m(s) \\ d_e(s) \end{bmatrix} = \mathbf{S}_O(s)\mathbf{P}_d(s)d(s). \quad (1)$$

We then define the attenuation factor as

$$\begin{aligned} \alpha(\omega) &\triangleq \frac{||y(j\omega)||_{CL}}{||y(j\omega)||_{OL}} \\ &= \frac{||\mathbf{S}_O(j\omega)\mathbf{P}_d(j\omega)||}{||\mathbf{P}_d(j\omega)||}. \end{aligned}$$

In the sequel we will show that there are situations, experienced in the setup [4] for which $\alpha(\omega)$ must be greater than one. First, we define the notion of alignment angles introduced in [9].

Definition 1: The *plant-controller alignment* angle (at frequency ω) is

$$\phi_{pc}(j\omega) \triangleq \cos^{-1}\left(\frac{|\mathbf{C}(j\omega)\mathbf{P}(j\omega)|}{||\mathbf{C}(j\omega||||\mathbf{P}(j\omega)||}\right) \quad (2)$$

while the *plant-disturbance alignment* angle is

$$\phi_{pd}(j\omega) \triangleq \cos^{-1}\left(\frac{|\mathbf{P}^H(j\omega)\mathbf{P}_d(j\omega)|}{||\mathbf{P}(j\omega||||\mathbf{P}_d(j\omega)||}\right). \quad (3)$$

The plant and controller (plant and disturbance) are said to be *perfectly aligned* if $\phi_{pc}(j\omega) = 0°$ ($\phi_{pd}(j\omega) = 0°$), and *completely misaligned* if $\phi_{pc}(j\omega) = 90°$ ($\phi_{pd}(j\omega) = 90°$). From [Proposition 9, 9], we have the following upper and lower bounds on the attenuation factor:

$$\begin{aligned} \alpha(\omega) \quad \leq \\ \sqrt{\sin^2\phi_{pd}(j\omega) + (\cos\phi_{pd}(j\omega)|S_I(j\omega)| + \sin\phi_{pd}(j\omega)|T_I(j\omega)|\tan\phi_{pc}(j\omega))^2} \end{aligned} \quad (4)$$

$$\begin{aligned} \alpha(\omega) \quad \geq \\ \sqrt{\sin^2\phi_{pd}(j\omega) + |\cos\phi_{pd}(j\omega)|S_I(j\omega)| - \sin\phi_{pd}(j\omega)|T_I(j\omega)|\tan\phi_{pc}(j\omega)|^2}. \end{aligned} \quad (5)$$

We now state the main result of this section. Its proof can be found in Appendix A.

Proposition 1: *If* $|y_e(j\omega)| = 0$ *and* $\phi_{pd}(j\omega_o) = 90°$, *then*

$$\frac{|y_m(j\omega)|}{||\mathbf{P}_d(j\omega)||} = \alpha(\omega) \geq \sqrt{1 + \left|\frac{P_{ed}(j\omega)}{P_{md}(j\omega)}\right|^2}. \quad (6)$$

From Proposition 1 we see that under perfect cancellation of $y_e(j\omega)$, $y_m(j\omega)$ must be amplified if the plant and disturbance transfer functions are completely misaligned. Furthermore, if $|P_{ed}(j\omega)| \gg |P_{md}(j\omega)|$, then $|y_m(j\omega)|$ could be unacceptably large[2].

Example 1: Using data from [4], we plot $\phi_{pd}(j\omega), \frac{|P_{ed}(j\omega)|}{|P_{md}(j\omega)|}$ and the lower bound (5) in Figure 4. At $\omega = 2\pi(174)$ rad/sec, $\phi_{pd}(j\omega) \approx 90°$, and $\frac{|P_{ed}(j\omega)|}{|P_{md}(j\omega)|}$ experiences its peak. From Proposition 1, we would then predict that the closed loop response $|y_m(j\omega)|$ is large. This is verified in Figure 5. Thus, while $|y_e(j\omega)|$ was attenuated in the closed loop, it appears to come at the expense of amplifying $|y_m(j\omega)|$.

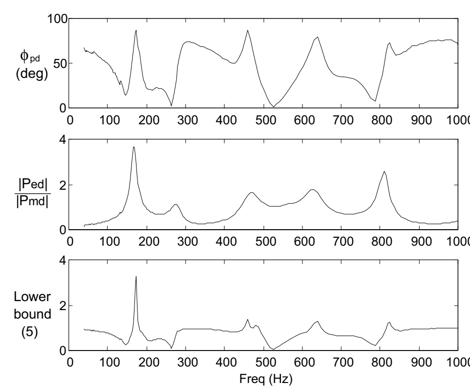

Figure 4: $\phi_{pd}(j\omega), \frac{|P_{ed}(j\omega)|}{|P_{md}(j\omega)|}$, and lower bound (5)

Remark 1: It is interesting to observe from Figures 4 and 5 that both $y_m(j\omega)$ and $y_e(j\omega)$ are small at frequencies where the plant and disturbance are well-aligned; i.e., $\phi_{pd}(j\omega) \approx 0°$. Clearly, at these frequencies both the upper bound (4) and lower bound (5) collapse to $|S_I(j\omega)|$ and the disturbance attenuation performance becomes a sensitivity minimization problem.

[2] For example, it may be unacceptable to have the disturbance amplified at any point in an HVAC system. The duct is a simplified model of such a system.

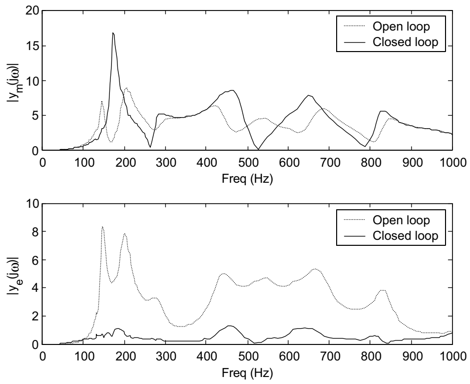

Figure 5: Open loop and closed loop comparison of $y_m(j\omega)$ and $y_e(j\omega)$

In other words, when $\phi_{pd}(j\omega) = 0°$, the disturbance affects the outputs in the same ay as does the control signal, and that this is favorable for disturbance rejection. Otherwise, one can only choose one of the two outputs for disturbance attenuation, and the control signal used to do so will act as a disturbance to the other output.

4 Stability margins

In the last section we concentrated on performance analysis and presented a situation where $|y_e(j\omega)|$ was attenuated at the expense of an amplified $|y_m(j\omega)|$. Specifically, we saw that $|y_m(j\omega)|$ peaks at the frequency where $\phi_{pd}(j\omega) \approx 90°$ and the ratio $\frac{|P_{ed}(j\omega)|}{|P_{md}(j\omega)|}$ has a maximum. So, we could expect a smaller stability margin (or a large $||\mathbf{S}_O(j\omega)||$) at this frequency. Therefore, our subsequent analysis will devote special attention to the condition $\phi_{pd}(j\omega) \approx 90°$ and $\frac{|P_{ed}(j\omega)|}{|P_{md}(j\omega)|} \gg 1$ occurring when $\omega = 2\pi(174)$ rad/sec . In this section we study the output sensitivity $\mathbf{S}_O(j\omega)$, whose size $||\mathbf{S}_O(j\omega)||$ provides one measure of stability margin; e.g. see [10].

Case 1: (feedforward only; $\mathbf{C}(j\omega) = [C_m(j\omega) \quad 0]$) In this case, the system's closed-loop response is given by

$$\mathbf{S}_O(j\omega) = \begin{bmatrix} S_I(j\omega) & 0 \\ -\frac{P_{eu}(j\omega)}{P_{mu}(j\omega)} T_I(j\omega) & 1 \end{bmatrix}. \tag{7}$$

Now, suppose $|y_e(j\omega)| = 0$. Then, from Lemmas 1 and 2 in Appendix A we have

$$|T_I(j\omega)| = \frac{|P_{ed}(j\omega)P_{mu}(j\omega)|}{|P_{md}(j\omega)P_{eu}(j\omega)|} \approx \left|\frac{P_{ed}(j\omega)}{P_{md}(j\omega)}\right|^2. \tag{8}$$

Thus, with $\frac{|P_{ed}(j\omega)|}{|P_{md}(j\omega)|} \gg 1$, it follows from the fundamental algebraic constraint $S_I(j\omega) + T_I(j\omega) = 1$ that $|S_I(j\omega)| \gg 1$. This in turn implies that $||\mathbf{S}_O(j\omega)|| \gg 1$. Thus, whenever we use only feedforward control, $\mathbf{C}(j\omega) = [C_m(j\omega) \quad 0]$, attenuation of $|y_e(j\omega)|$ at a frequency where both $\frac{|P_{ed}(j\omega)|}{|P_{md}(j\omega)|} \gg 1$ and plant-disturbance are misaligned necessarily leads to a reduced stability margin.

Case 2: (feedforward and feedback control; $\mathbf{C}(j\omega) = [C_m(j\omega) \quad C_e(j\omega)]$) Using straightforward manipulations, the output sensitivity and complementary sensitivity functions can be written as

$$\mathbf{S}_O(s) = \mathbf{I} - S_I(s)\mathbf{L}_O(s)$$

and

$$\mathbf{T}_O(s) = S_I(s)\mathbf{L}_O(s)$$

where

$$\mathbf{S}_O(j\omega) = \begin{bmatrix} S_{O11}(j\omega) & -\frac{P_{mu}(j\omega)}{P_{eu}(j\omega)} T_{O22}(j\omega) \\ -\frac{P_{eu}(j\omega)}{P_{mu}(j\omega)} T_{O11}(j\omega) & S_{O22}(j\omega) \end{bmatrix} \tag{9}$$

and where $S_{Oij}(j\omega)$ and $T_{Oij}(j\omega)$ are the (i,j)th element of $\mathbf{S}_O(j\omega)$ and $\mathbf{T}_O(j\omega)$, respectively. Note the similarities and differences to (7). The proof of the next propositon can be found in Appendix B.

Proposition 2: *If* $|y_e(j\omega)| = 0$*, then*

$$|T_{O11}(j\omega)| = \frac{\left|\frac{P_{mu}(j\omega)}{P_{eu}(j\omega)}\right|}{\left|\frac{P_{md}(j\omega)}{P_{ed}(j\omega)} + \frac{C_e(j\omega)}{C_m(j\omega)}\right|}. \tag{10}$$

Proposition 2 shows that for perfect cancellation, $|T_{O11}(j\omega)|$ depends not only on plant and disturbance transfer functions but also on both controllers. Therefore, unlike Case 1, the ratio $\frac{|P_{mu}(j\omega)|}{|P_{eu}(j\omega)|}$ does not impose a constraint on $|T_{O11}(j\omega)|$ when $y_e(j\omega) = 0$.

Since $S_{O11}(j\omega) + T_{O11}(j\omega) = 1$, then $|T_{O11}(j\omega)| \gg 1$ implies $|S_{O11}(j\omega)| \gg 1$, which, in using (9), leads to $||\mathbf{S}_O(j\omega)|| \gg 1$ and small stability margins. Note also that $|T_{O11}(j\omega)| \gg 1$ implies poor robust stability to multiplicative uncertainty in P_{mu}.

Example 2: Returning to the experiments in [4], we plot the magnitude ratios $\frac{|P_{mu}(j\omega)|}{|P_{eu}(j\omega)|}$ and $\frac{|P_{ed}(j\omega)|}{|P_{md}(j\omega)|}$ in Figure 6. The magnitude of each element of the output sensitivity $\mathbf{S}_O(j\omega)$ is shown in Figure 7 for the case $\mathbf{C}(j\omega) = [C_m(j\omega) \quad 0]$. At $\omega = 2\pi(174)$ rad/sec, $\phi_{pd}(j\omega) \approx 90°$ (see Figure 4), and $\frac{|P_{ed}(j\omega)|}{|P_{md}(j\omega)|} = 3.7$ (from Figure 6). So, by (8), $|T_I(j\omega)| \approx (3.7)^2 = 13.7$. From the algebraic constraint, $|S_I(j\omega)|$ is commensurately large. The data yields $||\mathbf{S}_O|| \approx 13$, which compares favorably with the preceeding analysis.

Now consider $\mathbf{C}(j\omega) = [C_m(j\omega) \quad C_e(j\omega)]$. Figure 8 shows the magnitude of the four elements of $\mathbf{S}_O(j\omega)$.

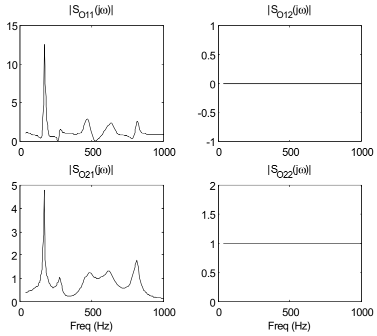

Figure 6: Magnitude plots of $\mathbf{S}_O(j\omega)$ for case $\mathbf{C}(j\omega) = [C_m(j\omega)\ \ 0]$

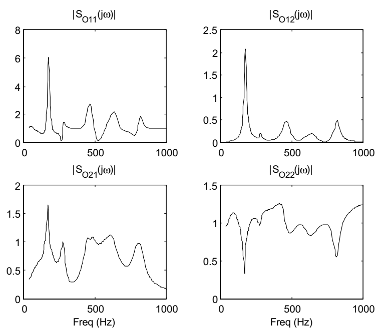

Figure 7: Magnitude plots of $\mathbf{S}_O(j\omega)$ for case $\mathbf{C}(j\omega) = [C_m(j\omega)\ \ C_e(j\omega)]$

We can compute $|T_{O11}(j\omega)|$ directly using Proposition 2, though it is easier to see from (9) that $|T_{O11}(j\omega)| = \frac{|P_{mu}(j\omega)|}{|P_{eu}(j\omega)|}|S_{O21}(j\omega)|$. At $\omega = 2\pi(174)$ rad/sec, the data from Figure 6 and Figure 8 gives $\frac{|P_{eu}(j\omega)|}{|P_{mu}(j\omega)|} = 0.4$ and $|S_{O21}(j\omega)| = 1.7$, resulting in $|T_{O11}(j\omega)| = \frac{1.7}{0.4} = 4.25$. This implies that the size of $|S_{O11}(j\omega)|$ is comparable. This is confirmed in Figure 8, where $|S_{O11}(j\omega)| = ||\mathbf{S}_O|| \approx 6$; a significant improvement over $||\mathbf{S}_O|| \approx 13$ using just feedforward control.

5 Conclusions

In this paper we have analyzed stability and performance of ANC in a duct using the SITO formulation. We derived a lower bound on closed-loop sound pressure level that depends only on open-loop transfer functions. We proved that using only feedforward controller imposes inherent limitations on the achievable closed-loop performance. We also show that this limitation, in terms of stability margin, can be alleviated when both feedforward and feedback controllers are used. At this point we have not discussed how to design the controllers to achieve the performance objective. This will be a topic for further research. Another interesting research direction is to study the relation of plant - disturbance alignment angle to the sensor and actuator configurations so that we can choose the setup that gives the best overall performance.

6 Appendices

A. Proof of Proposition 1: First we need some lemmas.

Lemma 1: *Given ω, $y_e(j\omega) = 0$ if and only if*

$$T_{O21}(j\omega) - \left(1 - \frac{P_{eu}(j\omega)}{P_{mu}(j\omega)}T_{O12}(j\omega)\right)\frac{P_{ed}(j\omega)}{P_{md}(j\omega)} = 0. \tag{11}$$

For the special case when $C_e(j\omega) = 0$:

$$T_I(j\omega) = \frac{P_{ed}(j\omega)P_{mu}(j\omega)}{P_{md}(j\omega)P_{eu}(j\omega)}. \tag{12}$$

Proof: From (1) we have

$$y_e(j\omega) = S_{O21}(j\omega)P_{md}(j\omega) + S_{O22}(j\omega)P_{ed}(j\omega)$$
$$= -T_{O21}(j\omega)P_{md}(j\omega) + (1 - T_{O22}(j\omega))P_{ed}(j\omega)$$
$$= -T_{O21}(j\omega)P_{md}(j\omega) + \left(1 - \frac{P_{eu}(j\omega)}{P_{mu}(j\omega)}T_{O12}(j\omega)\right)P_{ed}(j\omega).$$

Letting $y_e(j\omega) = 0$ yields (11). Equation (12) follows from $C_e = 0$ which, in turn, implies $T_{O12}(j\omega) = 0$ and $T_{O21}(j\omega) = \frac{P_{eu}(j\omega)}{P_{mu}(j\omega)}T_I(j\omega)$. □

Lemma 2: *Suppose $\phi_{pd} = 90^\circ$. Then,*

$$\frac{\overline{P}_{mu}(j\omega)}{\overline{P}_{eu}(j\omega)} = -\frac{P_{ed}(j\omega)}{P_{md}(j\omega)} \tag{13}$$

and

$$\frac{|P_{mu}(j\omega)|}{|P_{eu}(j\omega)|} = \frac{|P_{ed}(j\omega)|}{|P_{md}(j\omega)|} \tag{14}$$

independent of the controller[3].

Proof: Substitute $\phi_{pd} = 90^\circ$ into (3). □

We need the following notation (see [9]) for stating Lemma 3:

$$\begin{aligned}
\vec{\mathbf{P}}(j\omega) &\triangleq \mathbf{P}(j\omega)/||\mathbf{P}(j\omega)|| \\
\vec{\mathbf{P}}^{\perp}(j\omega) &\triangleq [-p_2(j\omega)\quad p_1(j\omega)]/||\mathbf{P}(j\omega)|| \\
\vec{\mathbf{C}}(j\omega) &\triangleq \mathbf{C}(j\omega)/||\mathbf{C}(j\omega)|| \\
\vec{\mathbf{C}}^{\perp}(j\omega) &\triangleq [-c_2(j\omega)\quad c_1(j\omega)]^T/||\mathbf{C}(j\omega)|| \\
\tan\phi_{pc}(j\omega) &\triangleq \frac{|\vec{\mathbf{C}}^{\perp H}(j\omega)\vec{\mathbf{P}}(j\omega)|}{|\vec{\mathbf{C}}(j\omega)\vec{\mathbf{P}}(j\omega)|} \\
&\triangleq \frac{|\vec{\mathbf{C}}(j\omega)\vec{\mathbf{P}}^{\perp H}(j\omega)|}{|\vec{\mathbf{C}}(j\omega)\vec{\mathbf{P}}(j\omega)|}
\end{aligned}$$

[3] Overbar denotes complex conjugate.

Lemma 3: *Suppose $\phi_{pd} = 90^\circ$ and $y_e(j\omega) = 0$. Then,*

$$|T_I(j\omega)| \tan\phi_{pc}(j\omega) = \frac{|P_{ed}(j\omega)|}{|P_{md}(j\omega)|}. \tag{15}$$

Proof: We will only show for the more general case $\mathbf{C}(j\omega) = [C_m(j\omega) \quad C_e(j\omega)]$. The situation $\mathbf{C}(j\omega) = [C_m(j\omega) \quad 0]$ would then follow directly by setting $C_e(j\omega) = 0$. The statement in Lemma 3 is equivalent to

$$y_e(j\omega) = 0, \;\; \phi_{pd} = 90^\circ$$
$$\Rightarrow \left| |T_I(j\omega)| \tan\phi_{pc}(j\omega) - \left|\frac{P_{ed}(j\omega)}{P_{md}(j\omega)}\right| \right| = 0.$$

To simplify notation, the dependence on ω is omitted. Then,

$$\begin{aligned} |T_I| \tan\phi_{pc} &= |T_I| \frac{|\vec{\mathbf{C}}\vec{\mathbf{P}}^{\perp H}|}{|\vec{\mathbf{C}}\vec{\mathbf{P}}|} = |T_I| \frac{|-C_m\bar{P}_{eu} + C_e\bar{P}_{mu}|}{|C_m P_{mu} + C_e P_{eu}|}; \\ |T_I| \tan\phi_{pc} &= \left| -\frac{\bar{P}_{eu}}{P_{eu}} T_{O21} + \frac{\bar{P}_{mu}}{P_{mu}} T_{O12} \right|. \end{aligned}$$

Therefore,

$$\left| |T_I| \tan\phi_{pc} - \left|\frac{P_{ed}}{P_{md}}\right| \right| =$$
$$\left| \left| -\frac{\bar{P}_{eu}}{P_{eu}} T_{O21} + \frac{\bar{P}_{mu}}{P_{mu}} T_{O12} \right| - \left|\frac{P_{ed}}{P_{md}}\right| \right|.$$

Applying Lemma 1 and rearranging terms gives

$$\left| |T_I| \tan\phi_{pc} - \left|\frac{P_{ed}}{P_{md}}\right| \right| =$$
$$\left| \left| -\frac{\bar{P}_{eu}}{P_{eu}}\frac{P_{ed}}{P_{md}} + \left(\frac{\bar{P}_{eu}}{P_{mu}}\frac{P_{ed}}{P_{md}} + \frac{\bar{P}_{mu}}{P_{mu}}\right) T_{O12} \right| - \left|\frac{P_{ed}}{P_{md}}\right| \right|.$$

Now ,at $\phi_{pd} = 90^\circ$, we use Lemma 2 to obtain

$$\left| |T_I| \tan\phi_{pc} - \left|\frac{P_{ed}}{P_{md}}\right| \right| =$$
$$\left| \left| \frac{\bar{P}_{eu}}{P_{eu}}\frac{\bar{P}_{mu}}{\bar{P}_{eu}} + \left(-\frac{\bar{P}_{eu}}{P_{mu}}\frac{\bar{P}_{mu}}{\bar{P}_{eu}} + \frac{\bar{P}_{mu}}{P_{mu}}\right) T_{O12} \right| - \left|\frac{P_{mu}}{P_{eu}}\right| \right|$$
$$= \left| \left|\frac{\bar{P}_{mu}}{P_{eu}}\right| - \left|\frac{P_{mu}}{P_{eu}}\right| \right| = 0.$$

□

We can now prove Proposition 1. Without loss of generality, assume $|d(j\omega)| = 1$. From (1), $y_e(j\omega) = 0$ implies

$$\frac{|y_m(j\omega)|}{||\mathbf{P}_d(j\omega)||} = \frac{||\mathbf{S}_O(j\omega)\mathbf{P}_d(j\omega)||}{||\mathbf{P}_d(j\omega)||} = \alpha(\omega).$$

Applying Lemma 3 and $\phi_{pd} = 90^\circ$ to the lower bound (5) gives

$$\alpha(\omega) \geq \sqrt{1 + \left|\frac{P_{ed}(j\omega)}{P_{md}(j\omega)}\right|^2}$$

and (6) follows. □

B. Proof of Proposition 2: Since $T_{O11} = \frac{P_{eu}}{P_{mu}} T_{O21}$, then,

$$\begin{aligned} T_{O11} &= \left(1 - \frac{P_{eu}}{P_{mu}} T_{O12}\right) \frac{P_{ed}}{P_{md}} \frac{P_{mu}}{P_{eu}} \\ &= \left(1 - \frac{C_e P_{eu}}{C_m P_{mu}} T_{O11}\right) \frac{P_{ed}}{P_{md}} \frac{P_{mu}}{P_{eu}}. \end{aligned}$$

Rearranging gives

$$\left(1 + \frac{C_e P_{ed}}{C_m P_{md}}\right) T_{O11} = \frac{P_{ed}}{P_{md}} \frac{P_{mu}}{P_{eu}}$$

and (10) follows. □

References

[1] S.M. Kuo and D. R. Morgan, *Active Noise Control Systems*, Wiley-Interscience, New York, 1996.

[2] P.A. Nelson and S. J. Elliott, *Active Control of Sound*, Academic Press, London, 1992.

[3] P.G. Metha, Y. Zheng, C.V. Hollot and Y. Chait, "Active Noise Control in Ducts: Feedforward/Feedback Design by Blending H_∞ and QFT Methods," *Proceedings of the 13th IFAC World Congress*, San Francisco, 1996.

[4] T. Klawitter, *Linear Active Duct Noise Control: Feedforward/Feedback Controllers Designed with H_∞ and Quantitative Feedback Theory,* M.S. Thesis, University of Massachusetts, Amherst, 2000.

[5] L. Li, *Experimental Inverstigation of LTI Feedforward Active Noise Control Design From Experimental Frequency Responses,* M.S. Thesis, University of Massachusetts, Amherst, 1999.

[6] P.G. Metha, *Fixed-Filter Designs for Active Noise Control in Ducts,* M.S. Thesis, University of Massachusetts, Amherst, 1996.

[7] A.J. Hull, C.J. Radcliffe, and S. C. Southward, "Global Active Noise Control of a One Dimensional Acoustic Duct Using a Feedback Controller," *J. Dyn. Sys. Meas. Contr.*, Vol. 115, pp. 488 - 494, 1993.

[8] J. Hong and D.S. Bernstein, "Bode Integral Constraints, Colocation, and Spillover in Active Noise and Vibration Control," *IEEE Trans. Control Systems Technology*, Vol. 6(1), pp. 111-120, 1998.

[9] J.S. Freudenberg and R.H. Middleton, "Properties of Single Input, Two Output Feed back Systems," *International Journal of Control*, Vol. 72(16) pp. 1446-1465, 1999.

[10] J.S. Freudenberg, C.V. Hollot, and D.P.Looze, *"A First Graduate Course in Feedback Control,"* Course Notes, EECS 565, University of Michigan, Winter, 2000.